Section A-Research paper

Radiographic features of Osteoid Osteoma

Mohamed M.A. Zaitoun, Ayman Fathy Zeid, Dina Abdelhamid Ali Mohamed, Ibrahim M. Eladl

Radiodiagnosis Department, Faculty of Medicine, Zagazig University, Egypt

Email: abdelhamiddina5@gmail.com

Article History: Received 10th June, Accepted 5th July, published online 10th July 2023

Abstract

Background: The radiographic appearance of osteoid osteoma depends on its site within the involved bone. There are three subtypes based on site: cortical, medullary, and sub-periosteal. Cortical lesions represent approximately 75% of osteoid osteomas, medullary lesions represent approximately 20% of tumors, and subperiosteal osteoid osteomas represent fewer than 5% of lesions. The sclerosis is reactive and does not represent the lesion itself. Radiographs characteristically show a circular ovoid cortical lucency representing the nidus (usually less than 1.5 cm in diameter) with a variable degree of surrounding sclerosis. sclerosis is extensive, it may interfere with visualization of the radiolucent nidus. Intramedullary and subperiosteal lesions may not demonstrate significant sclerosis, and the cortex overlying the site may appear normal, making intraoperative surgical localization difficult. Plain radiography is the first line of bone imaging. May appear normal and may show cortical thickening surrounding a solid periosteal reaction. The nidus may appear as a well-defined lucent region with a central dot of sclerosis. CT is the modality of choice and is excellent at characterizing the lesion. The most common appearance is a cortical-based lucency measuring less than 2 cm. Technetium-99–labeled MDP bone scintigraphy may be useful for confirming an osteoid osteoma diagnosis. The sensitivity of skeletal scintigraphy for detection is virtually 100%. Surgeons have used intraoperative gamma cameras both to locate tumors and to confirm resection. Pathologists have also used radionuclide studies to locate the nidus, thus facilitating histopathologic evaluation. On ultrasound, at intra-articular lesions, there will be a focal area of cortical irregularity and adjacent hypoechoic synovitis. The nidus can show hypoechogenicity with posterior acoustic enhancement. Ultrasound can detect hypervascularity of the nidus with Doppler assessment. Magnetic Resonance Imaging (MRI) is non-specific although being sensitive to marrow changes, it is usually unable to identify the nidus. The hyperemia and resultant bone marrow edema pattern may result in the scans being misdiagnosed as representing aggressive pathology. The MRI appearance of the nidus is variable. Most commonly, the tumor exhibits low to intermediate T1-weighted signals and heterogeneously high signal on T2-weighted and STIR sequences.

Keywords: Radiographic features of Osteoid Osteoma

DOI: 10.53555/ecb/2023.12.Si12.233

Introduction

Osteoid osteomas represent 10% of all benign bone tumors and 2– 3% of all primary bone tumors with a strong male predominance (M: F 2- 4:1). They usually affect children and young adults between the ages of 5 and 25 years. Classically the most common symptom is bone pain, which often worsens at night. Pain is described as a dull ache, but it may progress to severe localized pain over the site of the tumor. The pain is most caused by the release of prostaglandins; thus, it is relieved by aspirin or other non-steroidal anti-inflammatory drugs. **(1)**

1. Plain Radiography

The radiographic appearance of osteoid osteoma depends on its site within the involved bone. There are three subtypes based on site: cortical, medullary, and sub-periosteal. Cortical lesions represent approximately 75% of osteoid osteomas, medullary lesions represent approximately 20% of tumors, and subperiosteal osteoid osteomas represent fewer than 5% of lesions. **(2)**

The sclerosis is reactive and does not represent the lesion itself. The nidus is usually <2 cm in diameter, is typically ovoid and has a central region of mineralization. Radiographs characteristically show a circular ovoid cortical lucency representing the nidus (usually less than 1.5 cm in diameter) with a variable degree of surrounding sclerosis. sclerosis is extensive, it may interfere with visualization of the radiolucent nidus. Intramedullary and subperiosteal lesions may not demonstrate significant sclerosis, and the cortex overlying the site may appear normal, making intraoperative surgical localization difficult. **(3)**

2. CT

CT is the modality of choice and is excellent at characterizing the lesion. The most common appearance is a cortical-based lucency measuring less than 2 cm. The radiolucent nidus may show central calcification. The nidus is surrounded by fusiform sclerosis involving one side of a long bone diaphysis, especially the femur and tibia. With cortical lesions, the nidus is centrally located within reactive sclerosis, either contained within the primary cortex or oriented toward its endosteal or periosteal aspect. This reactive cortical thickening may be so deep as to obscure the nidus. Epiphyseal and metaphyseal tumors may show minimal sclerosis surrounding the nidus compared to the diaphysis. In contrast to cortical lesions, medullary osteoid osteomas typically cause mild-to-moderate eccentric sclerosis. Subperiosteal lesions manifest as soft-tissue masses adjacent to the affected bone and often do not produce reactive sclerosis. The bone subjacent to subperiosteal lesions shows irregular bony resorption. Medullary and subperiosteal tumors are most common within the femoral neck and in the hands and feet. These two subgroups are also the most common in intra-articular or juxta-articular locations. **(4)**

Thin-section CT (1–2-mm slices) reconstructed in bone algorithm with multiplanar reformats is optimal. CT is often helpful when the suspected nidus is obscured by surrounding sclerosis on radiography. CT often shows nidus mineralization, which may be punctate, amorphous, or ring-like. CT has been better than plain tomography in detecting and accurately locating the nidus and is especially useful in evaluating those areas in which anatomy is complex, such as the spine, hips, and small joints**. (2)**

Dynamic contrast-enhanced CT has been reported to be useful in differentiating osteoid osteoma from bone cysts and chronic osteomyelitis, specifically Brodie. abscess. The tumor nidus shows rapid early arterial enhancement, typically more than 40 HU above the baseline unenhanced study. There is persistent intralesional venous phase enhancement, with gradual regress of contrast agent and return to baseline attenuation. Enhancement of perilesional arteries parallels nidus enhancement both in timing and degree of enhancement.
On the contrary, Brodie's abscesses and bone cysts are avascular. **(5)**

Regarding spinal osteoid osteomas, these lesions typically manifest as low-density nidi in the posterior elements. Reactive sclerosis of the ipsilateral pedicle, lamina, or transverse process may be present. They may be associated with painful scoliosis ipsilateral to the lesion secondary to paravertebral spasm**. (4)**

CT helps demonstrate the angle of approach especially to avoid an adjacent neurovascular bundle (if present). **(6)** Rarely, CT results may be falsely negative. On CT scans, the nidus of a cortical or cancellous osteoid osteoma is a well-defined oval lesion of decreased attenuation, with a variable amount of surrounding sclerosis, ranging from mild sclerosis to extensive periosteal new bone. On macroscopic examination, however, the periphery of the nidus is irregular due to the coarse host lamellar bone, which circumscribes and sharply demarcates the lesion. **(5)**

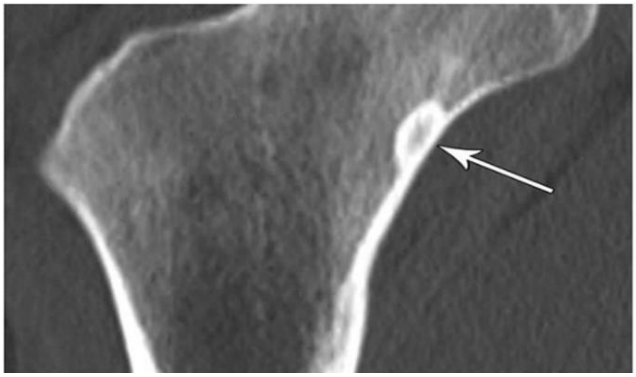

Fig. (1): Coronal reformatted CT image shows a cortically based sclerotic lesion (arrow), a finding consistent with a diagnosis of osteoid osteoma. **(6)**

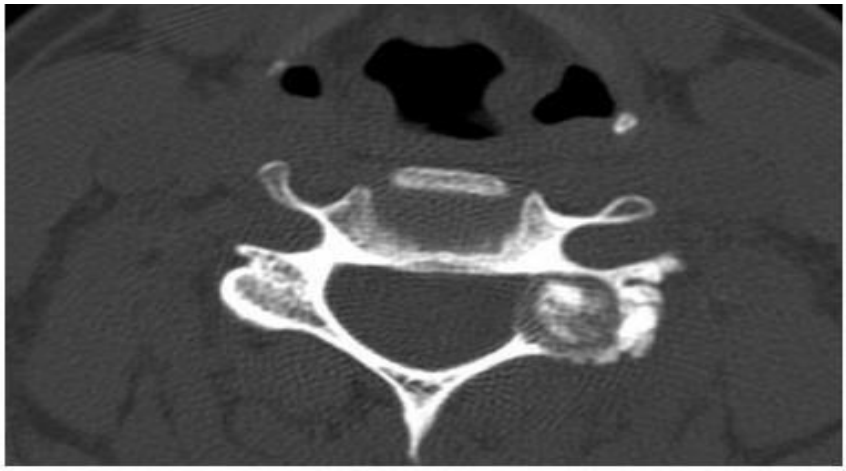

Fig. (2): Spinal osteoid osteoma. Axial CT image of the cervical spine in a 32-year-old woman demonstrates a 1.4-cm osteoid osteoma in the region of the left inferior articular process with mild narrowing of the left lateral recess. The lesion is too close to nerve roots and the cervical spinal cord to be treated with MW ablation. **(2)**

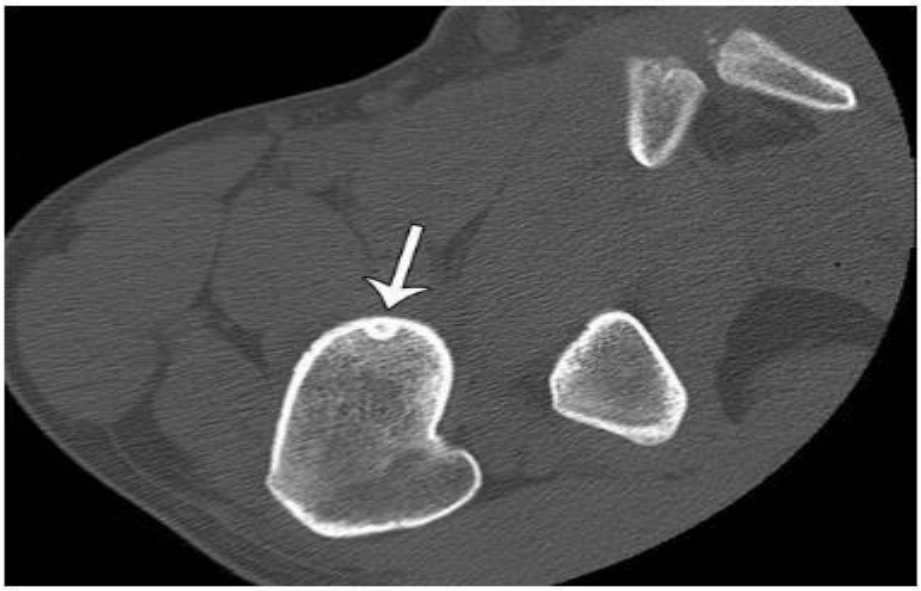

Fig. (3): Lesion localization in a 17-year-old boy. Axial thin-section CT image obtained with the leg in external rotation to facilitate needle placement clearly depicts an osteoid osteoma with radiolucent nidus(arrow) in the femoral neck. **(6)**

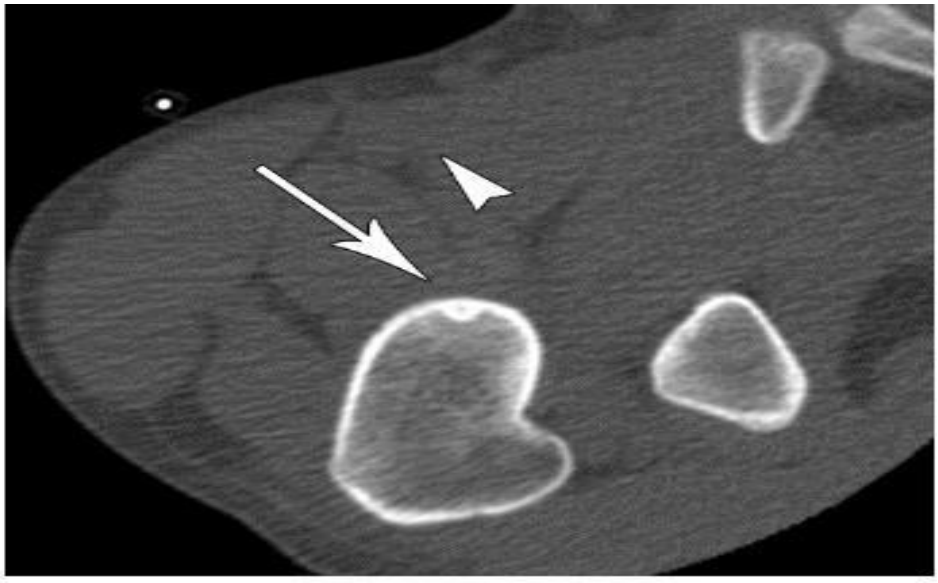

Fig. (4): Axial `CT image of the proximal femur demonstrates the preferred angle of approach, nearly perpendicular to the cortical surface (arrow). This approach was planned to avoid an adjacent neurovascular bundle (arrowhead). **(6)**

3. Nuclear medicine

Technetium-99–labeled MDP bone scintigraphy may be useful for confirming an osteoid osteoma diagnosis. The sensitivity of skeletal scintigraphy for detection is virtually 100%. Surgeons have used intraoperative gamma cameras both to locate tumors and to confirm resection. Pathologists have also used radionuclide studies to locate the nidus, thus facilitating histopathologic evaluation. **(7)**

The standard scintigraphy finding is the double-density sign on bone scan (also known as the less catchy hotter spot within hot area sign) which is highly specific and helpful in differentiating it from osteomyelitis. The central focus shows intense uptake within a surrounding lower uptake rim. Bone scintigraphy of osteoid osteoma typically shows focal radiotracer activity on both the immediate and delayed images. Scintigraphy is especially valuable in assessing osteoid osteoma in patients whose initial radiographs are negative or whose symptoms are atypical. Subsequent CT scans may be done based on the localization afforded by the scintigram. On scintigrams, intra-articular osteoid osteoma maydemonstrate diffuse distribution about the joint with a specific increase in tracer accumulation at the site of the nidus. (8)

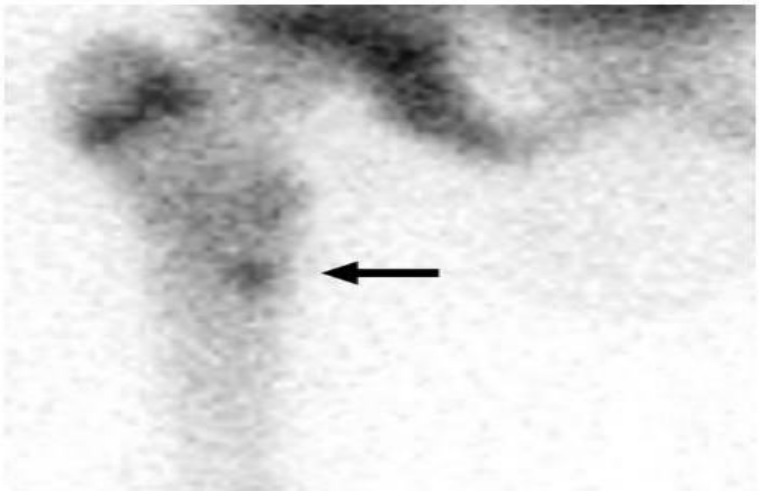

Fig. (5): Posterior spot image from technetium-99 bone M scan shows focal radiotracer uptake within nidus (arrow) and less-pronounced tracer uptake within the left femoral intertrochanteric region, illustrating scintigraphy double-density sign. **(8)**

4. PET

It can help in diagnosing osteoid osteoma and in post-therapy follow-up. It was reported that the tumor nidus exhibits 18FFDG–avid glucose metabolism, whereas the surrounding sclerosis does not. One month after percutaneous RFA, the nidus was no longer hypermetabolic. Many authors have also cited the benefit of SPECT for tumor diagnosis, particularly in the spine. (**9)**

5. Ultrasound

At intra-articular lesions, there will be a focal area of cortical irregularity and adjacent hypoechoic synovitis. The nidus can show hypoechogenicity with posterior acoustic enhancement. Ultrasound can detect hypervascularity of the nidus with Doppler assessment. **(10)**

6. MRI

It is non-specific although being sensitive to marrow changes, it is usually unable to identify the nidus. The hyperemia and resultant bone marrow edema pattern may result in the scans being misdiagnosed as representing aggressive pathology.

The MRI appearance of the nidus is variable. Most commonly, the tumor exhibits low to intermediate T1-weighted signal and heterogeneously high signal on T2-weighted and STIR sequences. **(7)** In a few cases, the nidus may present central calcifications, this might present as a low signal on both T1- and T2- weighted sequences. In contrast to MRI, tumor enhancement is variable; most lesions enhance diffusely as a result of their intrinsic vascularity however, heterogeneous rim enhancement may be seen. The surrounding osteosclerosis manifests as a fusiform low signal on both T1- and T2-weighted sequences. **(2)**

MRI may also depict edema within both perilesional bone marrow as well as surrounding soft tissues. Many studies have cited the superiority of CT over MRI in both diagnosing and characterizing osteoid osteomas.

Small lesions may be difficult to identify on MRI because the nidus signal is often similar to that of the surrounding cortex. (**9)**

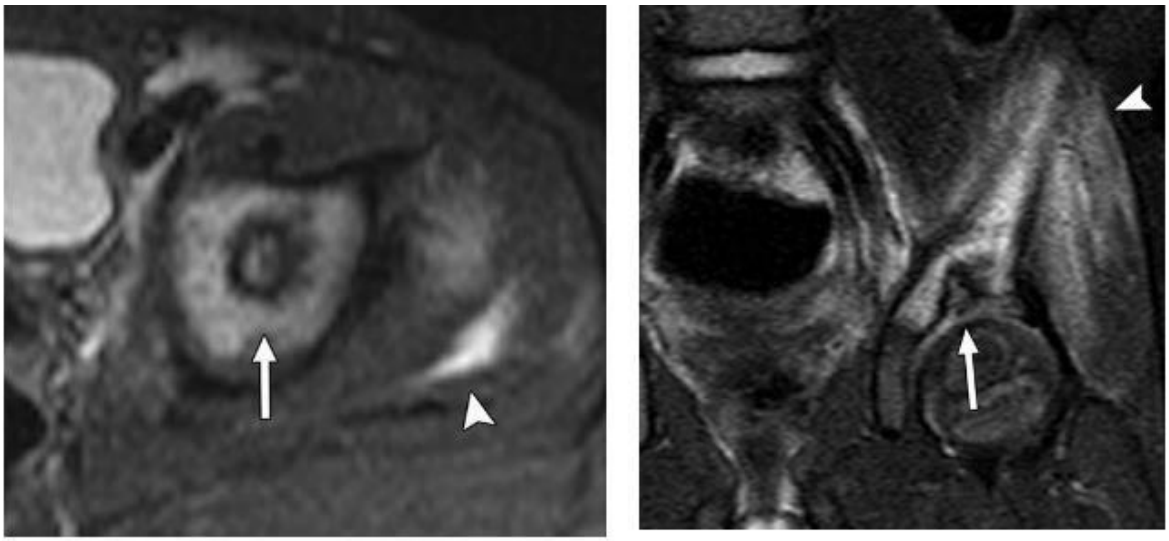

Fig. (6): A, B 3-year-old boy with left acetabular roof osteoid osteoma. Axial (A) and coronal (B) STIR images of the left hip depict intraarticular tumor (arrows) with predominantly high signal and thin low-signal margin. Note extensive edema (arrowheads) throughout the left ilium extending into the gluteus musculature **(7).**

Differential Diagnosis

Several conditions may exhibit features that mimic osteoid osteoma, including cortical thickening (osteomyelitis or muscle attachment), osteolysis, and marrow edema. Diagnostic considerations may include osteoblastoma, stress fracture, osteomyelitis, eosinophilic granuloma, bone cyst, avulsion fracture, chondroblastoma, intracortical hemangioma, and even well-differentiated osteosarcoma. **(11)**

For intra-articular or juxta-articular lesions, osteonecrosis, osteochondritis dissecans, and erosive

inflammatory arthritis may be considered. Osteoid osteomas and osteoblastomas overlap greatly in their clinical presentation, imaging manifestations, and even histologic appearance. As such, some authors classify both entities within the same family of osteoblastic tumors. **(12)**

Osteoblastomas are more expansile lesions with nidi that are typically larger than 1.5–2 cm and exhibit less perilesional sclerosis than osteoid osteomas. Unlike osteoid osteomas, osteoblastomas also grow over time and possess malignant potential. Clinically, osteoblastomas are less painful lesions and usually do not respond to salicylates to the same degree that osteoid osteomas do. Combining clinical history and a multimodality imaging approach typically results in correctly diagnosing osteoid osteoma. For example, stress fractures usually cause cortical thickening in a long bone diaphysis similar to tumors. However, fractures appear as a linear infraction in the center of the cortical thickening, whereas osteoid osteomas manifest as a round or oval lucency. Furthermore, on bone scintigraphy, stress fractures exhibit linear radiotracer uptake, whereas osteoid osteomas show the double-density sign. **(13)**

Differentiating intra-cortical abscesses from osteoid osteomas may be very difficult on conventional radiographs and unenhanced CT. When a sequestrum is present, the appearance of an abscess may closely mimic that of a calcified tumor nidus. Clinical information such as positive blood cultures or adjacent orthopedic hardware may strongly suggest infection. (**14)** Contrast-enhanced CT or MRI may also assist in diagnosis; abscesses will usually exhibit rim enhancement, whereas the vascular tumor nidus may enhance diffusely. In cases where the nidus shows rim enhancement, tissue diagnosis may be required to exclude osteomyelitis. **(2)**

Brodie abscess is one of the main differential diagnoses of osteoid osteoma, especially the cortical type. Although these two entities can be differentiated with CT, scintigraphy, and angiography. On CT scans, the inner surface of osteoid osteoma appears smooth, as does a central nidus whereas the peripheral margin of a Brodie's abscess is irregular, and if a sequestrum is present, it appears irregular and eccentric. On scintigrams, Brodie's abscess appears as an area of decreased radionuclide activity in the region of the nidus and the characteristic double-density sign will be of differentiating value. On angiograms, the necrotic center of a bone abscess is avascular, in contrast to the blush usually seen with osteoid osteoma. **(1)**

Osteoid osteoma is a painful benign bone tumor that occurs mainly in the lower extremities (femur and tibia) in young and adolescent male patients. The classic appearance in the radiograph is a radiolucent nidus with cortical thickening and surrounding sclerosis. Conventional radiographs, CT and scintigraphy are almost sufficient for the diagnosis of osteoid osteoma with proper clinical background. **(15)**

Treatment and prognosis

Treatment varies from just medical management with NSAIDs to percutaneous interventions, including RFA, MWA and surgical removal. Various imaging manifestations of osteoid osteomas increase its recognition and facilitate more rapid diagnosis and referral for treatment. **(16)**

Surgical resection has many potential complications, including difficult intraoperative identification of the tumor, local recurrence from incomplete resection, and resection of weight-bearing bone that can necessitate prolonged hospital stays and complicate recovery. **(17)**

Recently, CT-guided microwave ablation has developed as a less invasive alternative to surgical resection. In this technique, which can be performed under conscious sedation, an MWA probe is introduced into the tumor nidus through a cannulated needle under CT guidance and heat is applied locally to destroy tumor cells. Microwave ablation, first described in 2014, uses microwaves to ablate tumors thermally. A needle is inserted into the lesion under CT guidance and microwaves produced by the needle create a small heat region that heats and destroys the tumor. Microwave ablation is less affected by the type of tissue or tissue impedance than radiofrequency ablation. This method is highly successful. **(18)**

Treatment of osteoid osteoma by Microwave Ablation

Microwave Ablation (MWA) is defined as tumor destruction by devices with frequencies from 30 MHz to 30 GHz. **(19)**

Microwave ablation is the most developed technique in the Image **Guided Thermal Tumor Ablation**. The main advantages of microwave ablation, when compared with other thermo-ablative techniques, include persistently higher intra-tumoral temperatures, larger tumor ablation areas, faster ablation times, suitability for real-time imaging guidance, the capacity to do ablations in outpatient clinics, synergy with other cancer treatments, and repeatability and an increased convection profile. **(20)**

I. Physics of Microwaves

1. Microwave Radiation:

Microwave radiation is defined as the region of the electromagnetic spectrum with frequencies from 30 MHz to 30 GHz. This type of radiation is located between infrared radiation and radio waves. **(20)**

2. Mechanism of Heat Generation:

Water molecules (H2O) are dipolar; the charges on the atoms are such that the hydrogen side of the molecule has a positive charge, and the oxygen side has a negative charge. Electromagnetic radiation has an electric charge as well; the "wave" representation is the electric charge on the wave as it flips between positive and negative. For a microwave oscillating at 9.2x108Hz, the charge changes signs nearly 2 billion times a second. When an oscillating electric charge from radiation interacts with a water molecule, it causes the molecule to flip. Microwave radiation is specially tuned to the natural frequency of water molecules to maximize this interaction. As a result of the radiation hitting the molecules, the electrical charge on the water molecule flips back and forth 2-5 billion times a second depending on the frequency of the microwave energy. **(20)**

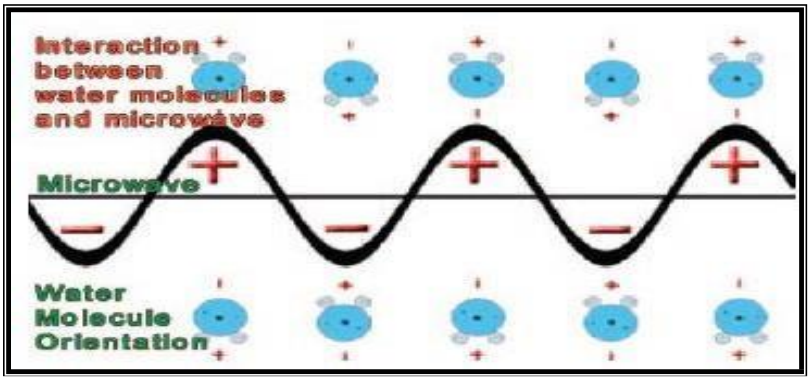

Fig. (7): Schematic illustrates the microwaves interaction **(20).**

3. Other Mechanisms of Heat Generation:

Another mechanism responsible for heat generation is ionic polarization which occurs when ions move in response to the applied electric field of the microwave. Displacement of ions causes collision with other ions, converting kinetic energy into heat. However, it is a neglected mechanism in comparison to dipole rotation in living tissue.

II- Microwave Ablation System

1) Historical Review of Microwave Systems:

The first microwave system used for Percutaneous MWA was the Microwave which had a needle antenna 1.6mm in diameter operating at 2,450 MHz.

In the early 1990s, MWA was used to treat hepatic tumors; but it was used in a few cases because it was only used in small ablation diameters due to its single 2.4 GHz needle antenna. This problem was solved with the introduction of multiple, clustered antennae, which allowed the ablation of bigger tumors.

2) Microwave System Components:

MWA systems consist of three basic elements: microwave generator, low-loss flexible coaxial cable and microwave antenna**.**

- ***Microwave Generator***

The microwave is generated by a magnetron. The magnetron contains spaces called resonant cavities which act as tuned circuits and generate electric fields. The microwave output frequency is also determined by the cavities. The antenna is connected via a low-loss coaxial cable to the microwave machine and transmits microwaves from the magnetron into the tissue. Most antennae are needle-like and are usually introduced into the tumor under imaging guidance**.**

Commercially available frequencies of microwave generators:

Recently, frequencies of 915 and 2,450 MHz have been used for MWA. All commercially available microwave systems are operating at either of the two frequencies. 2,450 MHz is more commonly used for MWA**.** There are two systems microwave-cooled and uncooled systems. This system implements smaller-sized probes at lower cost. The cooled most common one but uncooled can operate at significantly lower temperatures and may be preferred when high temperatures are undesired, such as in cases where vulnerable structures such as the thyroid gland are located close. This system, however, may also be used in osteoid tissue, creating an ablation zone almost similar in size by employing almost a quarter of the power**. (21)**

- ***Cable (Feeding Line)***

1. Coaxial Cable Line:

Most ablation antennas are connected to coaxial lines with small sizes and electromagnetic wave propagation. Their unbalanced design, however, allows return current flow on the outer conductor. These currents restrict impedance matching and may result in burning around the insertion point of the probe. If the antenna's input impedance is not matched to the feed line, too more of the applied energy is reflected from the antenna and, hence, not deposited in the tissue. The impedance mismatch results in standing waves that can increase the coaxial feed heat and lead it to fail ***(22)***

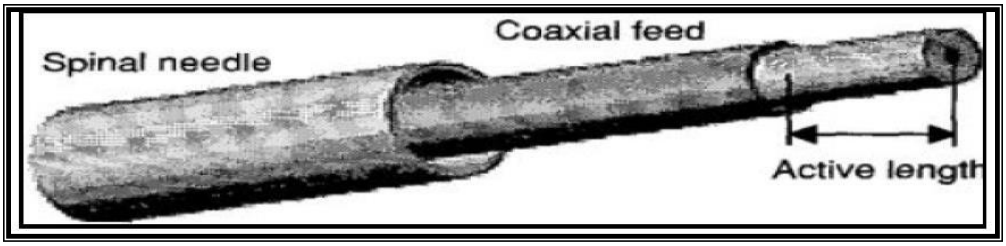

Fig. (8): Coaxial antenna inserted through a biopsy needle.

2. Newly Developed Triaxial Cable Line:

Triax cable provides a protective layer (driven guard) that exactly tracks SMU voltage sweep (force line). This removes cable charging since the inner and outer parts of the cable are usually kept at the same potential. This also removes any noise since the driven guard is connected to a separate low-noise amplifier. Never short the guard and force lines. This not only defeats the effect of the driven guard but may also shut down the SMU and generate a fatal error message.

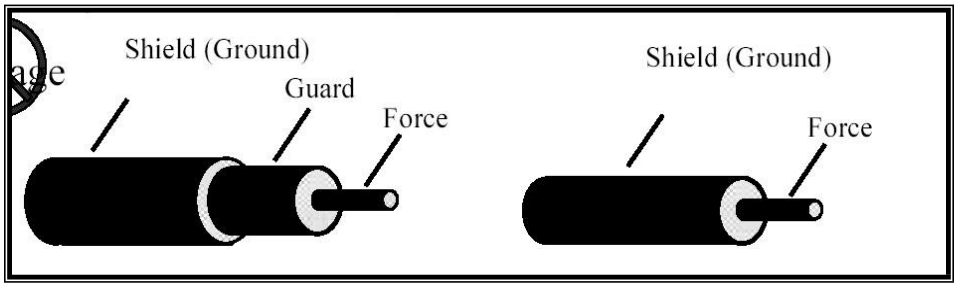

Fig. (9): Triax cable with an added layer (driven guard) that used to track SMU voltage sweep (force line).

- ***The Antenna***

These devices are often referred to as “needles” or other Nonspecific terms. Hence, the term applicator must be used in general to describe all devices. For precision, microwave applicators are **Antenna.**

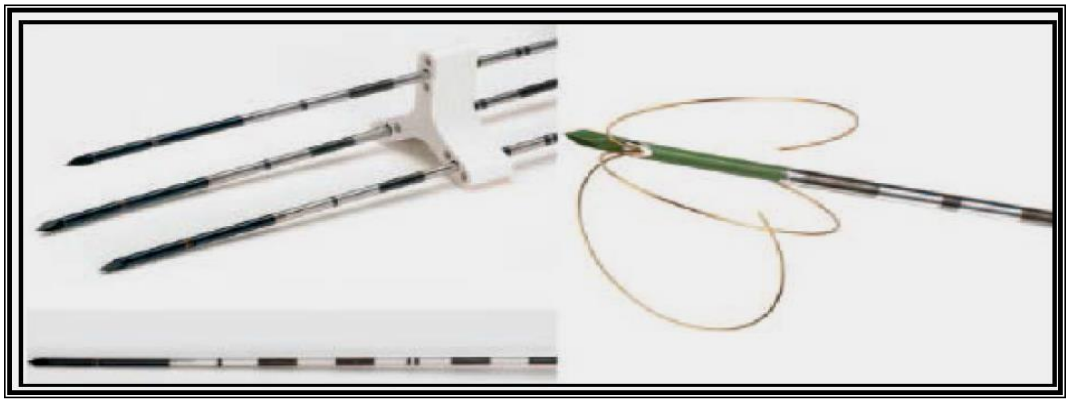

Fig. (10): Photographs reveal recent microwave antennas (single, multiple and loop) available for microwave tumor ablation. **(20)**

Classification of Antenna According to Configuration (Shape and Number):

1. Standard single-straight antenna configuration had a 13-gauge diameter, a 15cm length, and a 3.6 cm antenna tip.
2. A triangular triple-straight antennae configuration is formed with a rigid spacer that separates the three individual straight antennae by 1.5cm or 2.0cm.
3. The loop antenna that formed a cage consisted of three 13-gauge shafts, each with a wire-like antenna tip that was introduced into a circular loop after positioning in the target tissue. The three antenna loops, each 3cm in diameter, approximated a spherical cage to perform ablation of the circumscribed volume, as well as the margin of tissue outside the 3cm sphere**. (23)**

The choice of applicator gauge (14G, 17G, or 18G) relies on the amount of energy needed by the specific ablative treatment **(24)**

Indications of MWA

CT-guided MWA ablation should be attempted only when a definite nidus is identified on CT in a patient with an appropriate history suggestive of osteoid osteoma. The target tissue is the nidus. Strict criteria comprising visualization of a distinct radiolucent, round, or oval nidus with variable internal calcification on fine-section CT (slice thickness, 1- 3mm) should be applied. This will avoid the risk of ablating lesions that may mimic an osteoid osteoma such as a Brodie's abscess or geode, for which an alternative therapy or no treatment is required. **(25)**

Equipment

CT guidance affords the best available visualization of needle and probe placement within the lesion nidus. Helical CT with low-dose, "quick-check" CT fluoroscopy results in savings of time and dose for the patient. A general anesthetic allows a pain-free procedure and a stable patient position, although spinal anesthesia is an option for lower limb lesions. Early in our experience, local anesthetic proved unsuccessful because of inadequate pain control despite adequate anesthetic infiltration in soft tissue and overlying periosteum. Entering the nidus itself elicits extreme pain in most cases resulting in patient movement and loss of position.

The coaxial bone biopsy system is used for lesion access. The system's small-caliber needles and multi-capability components such as drill and biopsy cannula make it ideally suited for MWA ablation. The system comprises a 95-mm-long 14-gauge (2.1 mm) Bonopty Penetration cannula, a 100- mm-long 15-gauge (1.7 mm) Bonopty Drill, a 160-mm-long 15-gauge (1.7 mm) Bonopty Extended Drill and the 160-mm-long**.** For most patients with limb lesions, supine positioning is ideal because it affords good access and is the best position for the administration of a general anesthetic. The limb may be internally or externally rotated and secured with tape or straps to allow good skin access, easier needle placement and avoidance of neurovascular structures. Spinal lesions are treated with the patient lying prone with a padded ring beneath the chest for easier ventilation. A laser goniometer (Targo-Beam; Vasculab Medizintechnik, Wismar, Germany) can help guide accurate, first-time needle placement**. (26)**

Contraindications and limitations

Contraindications for these ablation techniques are rare but include lack of safe access, acute immunosuppression, local or systemic infection, uncorrected coagulopathy, pregnancy and patient refusal to consent. Relative contraindications include very large lesions and proximity to a sensitive structure that cannot be monitored or protected (the location of a lesion is less than 1 cm from vital structures such as nerves). In the spine, unstable fractures and metastatic epidural spinal cord compression are the most frequent relative contraindications. **(25)**

Potential Complications

Although this technique is minimally invasive, potential complications that may occur during needle passage include bleeding and nerve injury. These can be avoided by knowledge of anatomic structures in the region of needle passage and an alteration in the approach to avoid neurovascular bundles. Soft tissue burns, especially skin burns, are a further possible complication. There is a higher risk of skin necrosis in osteoid osteomas in superficially located bone, in which extra care is required. This complication is avoided by withdrawing the outer cannula to approximately 1 cm above the non-insulated tip of the coagulation cannula. Despite this precaution, we had data on one skin burn complication in a patient with an anterior tibial osteoid osteoma. The most likely explanation is a defect in the insulation material covering the thermal ablation cannula that was not confirmed as the cannula had been discarded immediately after the procedure. A quick visual check of the insulation material to avoid this rare occurrence is advised**. (27)**

References

1. Ferrao PN, Saragas NP, Strydom A, Tladi M. Osteoid osteoma of the hallux: a case report and review of the literature. SA Orthopaedic Journal. 2018; 17(4):52-6.
2. Bhure U, Roos JE, Strobel K. Osteoid osteoma: multimodality imaging with focus on hybrid imaging. European journal of nuclear medicine and molecular imaging. 2019; 46(4):1019-36
3. Ladd LM and Roth TD. Computed tomography and magnetic resonance imaging of bone tumors. Seminars in Roentgenology. 1-61.
4. Iyer RS, Chapman T, Chew FS. Pediatric bone imaging: diagnostic imaging of osteoid osteoma. American Journal of Roentgenology. 2012; 198(5):1039-52.
5. Holden DM, Ilaslan H, Sundaram M. An Imaging Approach to Bone Tumors. In: Tumors and Tumor- Like Lesions of Bone. Springer, London. 2015: 11-55.
6. Cuesta HE, Villagran JM, Horcajadas AB, Kassarjian A, Caravaca GR. Percutaneous radiofrequency ablation in osteoid osteoma: Tips and tricks in special scenarios. European journal of radiology. 2018; 102:169-75.
7. Whitmore MJ, Hawkins CM, Prologo JD, Marshall KW, Fabregas JA, Yim DB, Monson D, Oskouei SV, Fletcher ND, Williams RS. Cryoablation of osteoid osteoma in the pediatric and adolescent population. Journal of Vascular and Interventional Radiology. 2016; 27(2):232-7.
8. Infante JR, Lorente R, Rayo JI, Serrano J, Domínguez ML, García L, Moreno M. The use of radioguided surgery in the resection of osteoid osteoma. Revista Española de Medicina Nuclear e Imagen Molecular (English Edition). 2015; 34(4):225-9.
9. Noordin S, Allana S, Hilal K, Nadeem N, Lakdawala R, Sadruddin A, Uddin N. Osteoid osteoma: contemporary management. Orthopedic reviews. 2018; 10(3).
10. Leeman JJ, Motamedi D, Wildman-Tobriner B, O'Donnell RJ, Link TM. Intra-articular osteoid osteoma at the femoral trochlea treated with osteochondral autograft transplantation. Journal of radiology case reports. 2016; 10(6):22.
11. Lindquester WS, Crowley J, Hawkins CM. Percutaneous thermal ablation for treatment of osteoid osteoma: a systematic review and analysis. Skeletal radiology. 2020 Sep;49(9):1403-11.
12. Singh A and Solomon MC. Osteoid osteoma of the mandible: A case report with review of the literature. Journal of dental sciences. 2017; 12(2):185-9.
13. Zhang Y and Rosenberg AE. Bone-forming tumors. Surgical pathology clinics. 2017; 10(3):513-35.
14. Barbiera F, Murmura E, Murmura B, Accardi M, Botta A, Aiello A, La Grutta L, Lagalla R. Osteoid Osteoma: typical and atypical radiological findings. European Congress of Radiology-ECR 2018: 1- 10.
15. Claeys R, Walsdorff M, Pargov S, Matasa R, Duttmann R, Cannie M. Osteoid osteoma of the pisiform bone: a rare cause of wrist pain. Hand Surgery and Rehabilitation. 2016; 35(4):296-8.
16. May CJ, Bixby SD, Anderson ME, Kim YJ, Yen YM, Millis MB, Heyworth BE. Osteoid osteoma about the hip in children and adolescents. JBJS. 2019; 101(6):486-93.
17. Coluzzi F, Billeci D, Maggi M, Corona G. Testosterone deficiency in non-cancer opioid-treated patients. Journal of endocrinological investigation. 2018; 41(12):1377-88.
18. Kostrzewa M, Diezler P, Michaely H, Rathmann N, Attenberger UI, Schoenberg SO and Diehl SJ: Microwave ablation of osteoid osteomas using dynamic MR imaging for early treatment assessment: preliminary experience. J Vasc Interv Radiol 25(1): 106-111, 2014.
19. Goldberg SN, Charboneau JW, Dodd GD 3rd, et al., (2005): International Working Group on Image- Guided Tumor Ablation .Radiology; 228(2):335-45.
20. Simon CJ, Dupuy DE and Mayo-Smith WW. (2005): Microwave Ablation: Principles and Applications. Radiographics.
21. Yildirim G, Karakas HM, Gunkan A. uncooled microwave ablation method for thyroid nodules: our early-term results. Bosphorus Med J 2021;8:13–20.
22. Hines-Peralta AU, Pirani N, Clegg P, et al. Microwave ablation: results with a 2.45-GHz applicator in ex vivo bovine and in vivo porcine liver. Radiology. 2006; 239(1):94–102.
23. Shock SA, Meredith K, Warner TF, et al. Microwave ablation with loop antenna: in vivo porcine liver model. Radiology 2004;231:143–9.
24. Brace CL. Microwave ablation technology: what every user should know. Curr Probl Diagn Radiol. 2009; 38(2):61–67.

25. Prud'homme C, Nuefer JP, Runge M, Dubut J, Kastler B, Aubry S (2016) Prospective pilot study of CT-guided microwave ablation in the treatment of osteoid osteomas. Skeletal Radiol 46(3):315–323.

26. Furlow B. CT-guided interventional radiology. Radiologic technology. 2019; 90(6):581-597.

27. Finck CA, Zur Linden AR, Singh A, Foster RA, Nykamp SG, Sears WC. Effects of repeated use and resterilization on structural and functional integrity of microwave ablation antennas. American journal of veterinary research. 2017; 78(4):508-16.